CXCR4 blockade alleviates pulmonary and cardiac outcomes in early COPD

Isabelle Dupin[1,2], Pauline Henrot[1,2,3], Elise Maurat[1,2], Reshed Abohalaka[1,2], Sébastien Chaigne[1,2,3], Dounia El Hamrani[1,2], Edmée Eyraud[1,2], Renaud Prevel[1,2,3], Pauline Esteves[1,2], Maryline Campagnac[1,2], Marielle Dubreuil[1,2], Guillaume Cardouat[1,2], Clément Bouchet[1,2], Olga Ousova[1,2], Jean-William Dupuy[1,2], Thomas Trian[1,2], Matthieu Thumerel[1,2,3], Hugues Bégueret[1,2,3], Pierre-Olivier Girodet[1,2,3], Roger Marthan[1,2,3], Maeva Zysman[1,2,3], Véronique Freund-Michel[1,2], Patrick Berger[1,2,3]

[1] Univ. Bordeaux, Centre de Recherche Cardio-thoracique de Bordeaux, INSERM U1045, IHU Liryc, CIC 1401, Proteomics Facility, F-33600 Pessac, France

[2] INSERM, Centre de Recherche Cardio-thoracique de Bordeaux, U1045, CIC 1401, F-33600 Pessac, France

[3] CHU Bordeaux, Service d'exploration fonctionnelle respiratoire, Service de réanimation, Service de pneumologie, Service de chirurgie thoracique, Service de cardiologie-électrophysiologie et stimulation cardiaque, Service d'anatomopathologie, CIC-P 1401, F-33600 Pessac, France

Corresponding author: Prof. Isabelle Dupin

Centre de Recherche Cardio-thoracique de Bordeaux, INSERM U1045

PTIB. Hôpital Xavier Arnozan. Avenue du Haut Lévêque. 33600 Pessac

e-mail : isabelle.dupin@u-bordeaux.fr

Main Authors' contribution:

- conception and design (ID, PB)
- data acquisition (ID, PH, EM, RA, SC, DEH, EE, PE, MC, MD, GC, CB, OO, JWD, TT, VFM)
- data analysis (ID, PH, EM, RA, SC, DEH, RP, MD, GC, CB, JWD, VFM, PB)
- data interpretation (ID, PH, EM, RA, SC, DEH, EE, RP, PE, MD, GC, CB, TT, RM, MZ, VFM, PB)
- resources (PH, MC, MD, MT, HB, POG, MZ, PB)
- drafting the manuscript (ID, PH, PB)
- revision and final approval of the version to be published, agreement to be accountable for all aspects of the work in ensuring that questions related to the accuracy or integrity of any part of the work are appropriately investigated and resolved (All)

Source of support: the project was supported by a grant from the "Fondation de l'Université de Bordeaux" (Fonds pour les maladies chroniques nécessitant une assistance médico-technique FGLMR/AVAD) (ID), a grant from « Aquitaine Science Transfert » (PB) and AstraZeneca (an unrestricted grant to PB), the "Investments in the Future" program managed by the "Agence Nationale de la Recherche" (ANR, grant reference ANR-10-IAHU-04). The COBRA cohort was funded by AstraZeneca, Chiesi, Glaxo-SmithKline, Novartis, Chiesi,Roche and Legs Poix fondation.

Running head: CXCR4 blockade alleviates early COPD

This article has an online data supplement

Conflict of interest:

ID has 2 patents delivered (i) (EP N°3050574 *i.e.*, Use of plerixafor for treating and/or preventing acute exacerbations of chronic obstructive pulmonary disease); (ii) (EP N°20173595.8 *i.e.*, New compositions and methods of treating COVID-19 Disease). ID report a grant from the "Fondation Bordeaux Université," with funding from "Assistance Ventilatoire à Domicile" (AVAD) and "Fédération Girondine de Lutte contre les Maladies Respiratoires" (FGLMR).

PH reports non-financial support from AVAD and Chiesi, outside the submitted work and a grant from the "Fondation Bordeaux Université," with funding from AVAD and FGLMR.

POG reports grants, personal fees and non-financial support from AstraZeneca, personal fees and non-financial support from Chiesi, personal fees and non-financial support from GlaxoSmithKline, personal fees and non-financial support from Novartis, personal fees and non-financial support from Sanofi, outside the submitted work. POG has 2 patents delivered (i) (EP N°3050574 *i.e.*, Use of plerixafor for treating and/or preventing acute exacerbations of chronic obstructive pulmonary disease); (ii) (EP N°20173595.8 *i.e.*, New compositions and methods of treating COVID-19 Disease).

MZ reports personal fees from AstraZeneca, Boehringer Ingelheim, CSL Behring, Novartis, Chiesi, GlaxoSmithKline and non-financial support Lilly outside the submitted work and a grant from the "Fondation Bordeaux Université," with funding from AVAD and FGLMR.

PB is the medical coordinator of the French national cohort (*i.e.*, COBRA), which received grants from AstraZeneca, GlaxoSmithKine, Roche, Chiesi, Novartis and Legs Poix fundation. Moreover, PB reports grants and personal fees from Novartis, personal fees and non-financial support from Chiesi, grants, personal fees and non-financial support from Boehringer Ingelheim, personal fees and non-financial support from AstraZeneca, personal fees and non-financial support from Sanofi, personal fees from Menarini, personal fees from TEVA, outside the submitted work; in addition,

PB has 2 patents delivered (i) (EP N°3050574 *i.e.*, Use of plerixafor for treating and/or preventing acute exacerbations of chronic obstructive pulmonary disease); (ii) (EP N°20173595.8 *i.e.*, New compositions and methods of treating COVID-19 Disease). All other authors declare they have no competing interests.

ABSTRACT

Rationale: Chronic obstructive pulmonary disease (COPD) is a prevalent respiratory disease lacking effective treatment. Focusing on the early stage of COPD should help to discover disease modifying therapies. **Objectives**: In this study, we examined the role of the CXCL12/CXCR4 axis in both a mouse model of early COPD and in human samples from COPD patients. **Methods**: To generate the early COPD model, mice were exposed to cigarette smoke (CS) for 10 weeks and intranasal instillations of polyinosinic–polycytidylic acid (poly(I:C)) for 5 weeks to mimic exacerbations. **Measurements and Main Results**: Exposed mice presented mild airway obstruction, peri-bronchial fibrosis and right heart remodeling. CXCR4 expressing cells number was increased in the blood of exposed mice, as well as in the blood of patients with COPD. Lung CXCL12 expression was higher in both exposed mice and early COPD patients. The density of fibrocytes expressing CXCR4 was increased in the bronchial submucosa of exposed mice. Conditional inactivation of CXCR4 at adult stage as well as pharmacological inhibition of CXCR4 with plerixafor injections improved lung function, reduced inflammation and protected against CS and poly-(I:C)-induced airway and cardiac remodeling. $CXCR4^{-/-}$ and plerixafor-treated mice also had less CXCR4-expressing circulating cells and a lower density of peri-bronchial fibrocytes. **Conclusions**: We demonstrate that targeting CXCR4 has beneficial effects in an animal model of early COPD and provide a framework to translate these preclinical findings to clinical settings within a drug repurposing approach.

KEY WORDS: fibrocytes, bronchial remodeling, inflammation, obstruction, animal model

ABBREVIATIONS:

BAL	Broncho-alveolar lavage
bFGF	basic Fibroblast Growth Factor
BSM	Bronchial smooth muscle
CS	Cigarette smoke
CT	Computed tomographic
ECG	Electrocardiogram
FEV1	Forced expiratory volume in 1 second
FEV0.05	Forced expiratory volume in 0.05 second
FVC	Forced vital capacity
IFN	Interferon
LLN	Lower limit of normal
LV + S	Left ventricle plus septum
MRI	Magnetic Resonance Imaging
Poly-(I:C)	Polyinosinic–polycytidylic acid
RA	Room air
RV	Right ventricle
RVSP	Right ventricular systolic pressure
VEGF	Vascular Endothelial Growth Factor

INTRODUCTION

Chronic obstructive pulmonary disease (COPD) is a common disease, characterized by persistent respiratory symptoms and airflow limitation (1). Major risk factors for COPD include chronic exposure to noxious particles, mainly cigarette smoke (CS), and airway infections (2). Early COPD has been recently defined as patients aged <50 years with a smoking exposure >10 pack-years, with a ratio between forced expiratory volume in 1 second (FEV1) and forced vital capacity (FVC) less than 70% or less than the lower limit of normal (LLN), compatible computed tomographic (CT) abnormalities (*i.e.*, visual emphysema, air trapping, or bronchial thickening graded mild or worse), and/or evidence of accelerated FEV1 decline of >60 ml/years (3). Twenty-four percent of these early COPD patients developed clinical COPD 10 years later (4). A better understanding of this crucial phase for COPD development could help to tackle the disease before reaching irreversible tissue damage (5). However, it is very difficult to collect bronchial samples from these patients for research purpose, since they are pauci- or asymptomatic, demonstrating that we urgently need to develop animal models of early COPD.

Exposure of lung structural and immune cells to CS and infectious agents results in the release of various inflammatory substances, including chemokines (6). The chemokine receptor CXCR4 and its associated ligand CXCL12 appear to be attractive therapeutic targets for early COPD since: (i) they are implicated in the migration of inflammatory cells in COPD lungs (7), (ii) their expression and function are controlled by other cytokines (8), oxygen concentration (9) and microbial agents (10, 11), which are disrupted in COPD, and (iii) pharmacological blockade of CXCR4 reduces emphysema development in a long term COPD murine model (12).

CXCR4 is notably expressed by fibrocytes, a rare population of circulating fibroblast-like cells (13), that are assumed to play a crucial role in COPD. Indeed, blood fibrocytes are increased during

acute exacerbation of COPD implicating the CXCL12/CXCR4 axis, and related to higher mortality (7). Moreover, the bronchial density of fibrocytes is also increased in COPD and associated with worse functional outcomes (14).

In the present study, we thus hypothesized that the CXCL12/CXCR4 axis plays a role in the pathological processes leading to early COPD development and, hence, that inhibiting CXCR4 would protect from CS-induced airflow limitation and tissue remodeling. In a murine model of early COPD as well as COPD patients' tissues, both CXCR4-expressing cells in the blood and CXCL12 in the lung were upregulated. Using transgenic mice deficient for CXCR4 or the CXCR4 antagonist plerixafor, we showed that lungs were protected against CS-induced both lung function alteration and fibrocytes accumulation, and that the right heart was structurally resistant to cardiac remodeling, thus demonstrating a systemic effect of this therapeutic strategy.

METHODS

Complete details concerning methods appear in an online data supplement.

Study Population

Blood samples of COPD patients were obtained from "COBRA" (*i.e.*, COhort of BRonchial obstruction and Asthma; sponsored by INSERM) (Table E1) and human lung tissues from both the "Fibrochir" study (NCT01692444) (14) and "TUBE" (*i.e.*, TissUs Bronchiques et PulmonairEs, sponsored by the University hospital of Bordeaux) biological collection (Tables E2 and E3). All subjects gave their written informed consent to participate to the studies. The studies received approval from the local or national ethics committees.

Dataset transcriptomic analysis

Transcriptomes obtained on human blood and lung tissues were downloaded from the NCBI Gene Expression Omnibus (GEO) database (http://www.ncbi.nlm.nih.gov/geo/) using datasets under the accession codes of GSE100153 and GSE76925, respectively.

Mouse model of early COPD

Male C57BL/6J mice were obtained from Janvier (St Berthevin, France). $CXCR4^{lox/lox}$ and Cre2ERT2 mice were obtained from The Jackson Laboratory (15) and the "Institut Clinique de la Souris" (16), respectively. All animal studies were performed according to European directives for the protection of vertebrate animals. Agreement was obtained from French authorities (number A33-063-907) and all the protocols were approved by the local ethics committee.

Ten-week-old mice were exposed for 10 weeks to either room air (RA) or CS from non-filtered research cigarettes (2R4; University of Kentucky, Lexington, KY) using the smoking apparatus (Anitech, Paris, France), as described previously by Almolki *et al*. (17). After 5 weeks of CS exposure, mice were anesthetized and 50 µg of poly(I:C) diluted in PBS, mimicking responses by RNA virus infections (18), or its vehicle control, were administered twice per week for 5 weeks via nasal aspiration. Electrocardiograms (ECG) and Magnetic Resonance Imaging (MRI) were performed during the 10^{th} week of the protocol. After lung function measurement, right ventricular systolic pressure (RVSP) was determined invasively. Following bronchoalveolar lavage (BAL), mice were sacrificed and lung, heart and blood were collected. The Fulton index was calculated as the ratio between the right ventricle (RV) and the left ventricle plus septum (LV + S).

CXCR4 genetic deletion was induced by tamoxifen. CXCR4 pharmacological inhibition was induced by subcutaneous injection of 1 mg/kg plerixafor (Sigma-Aldrich, Saint-Quentin-Fallavier, France), 5 times/week during the last 5 weeks of the exposition protocol.

Experimental procedures in both human and mice

CXCR4-expressing cells were quantified in the blood and in the lungs by flow cytometry and immunohistochemistry, as described previously (14). CXCL12 and CXCR4 levels were evaluated by ELISA, western blotting and RT-PCR. Proteomics analyses were performed using mass spectrometry, as described previously (19).

Statistical Analysis

Statistical significance, defined as $P < 0.05$, was assessed by t-tests and MANOVA for variables with parametric distribution, and by Kruskal-Wallis with multiple comparison z tests, Mann-Whitney tests, Wilcoxon tests and Spearman correlation coefficients for variables with non-parametric distribution.

RESULTS

Chronic CS and poly(I:C) exposure induces functional obstruction, lung inflammation and both lung and heart tissue remodeling in mice

To model early COPD, we used a combination of CS exposure and intranasal instillations of poly(I:C). CS exposure for 5 weeks combined with 4 doses of poly(I:C) were not sufficient to trigger any functional airway obstruction (Figure E1A-D). In contrast, 10 weeks of CS exposure with 10 repeated instillations of poly(I:C) during the last 5 weeks (Figure 1A), significantly

decreased the FEV0.05/FVC ratio and increased the percentage of obstructive mice (Figure 1B-D). Other lung function parameters, particularly respiratory system compliance and tissue elastance, were not modified by CS and poly(I:C) exposure (Figure E1E-J). At the end of the 10 weeks exposure, the weight gain of the exposed mice was significantly different from that of the control mice (Figure E2A-B). CS and poly(I:C) exposure increased total cell count in the BAL fluid, as well as the absolute neutrophil, lymphocyte and macrophage numbers, 1 day after the last poly(I:C) instillation (d+1, Figure 1E-G). Although lower, the increase in neutrophils and lymphocytes persisted 4 days after the last poly(I:C) instillation (d+4, Figure 1E-G). CS and poly(I:C) synergistically enhanced airflow obstruction and BAL inflammation (Figure E3). We also analyzed lung proteomics obtained 1 day after the last poly-IC instillation. Of the 137 pathways that were significantly different in early COPD vs control mice, largest upregulated genes were those of the hypercytokinemia/ hyperchemokinemia box and of the pathogenesis of influenza and interferon (IFN) signaling (Figure 1H-I). In contrast, inhibited pathways were the wound healing and the xenobiotic metabolism PXR signaling pathways (Figure 1I). Finally, CS and poly(I:C)-exposed mice had a moderate but significant increase in peri-bronchial fibrosis compared to control mice (Figure 1J-K), mimicking the thickening of distal airway tissue in COPD patients (20).

Then, we investigated the impact of CS and poly(I:C) exposure on cardiac function. There was no evidence of heart failure in our model (Figure E4A-B). Moreover, there was no sign of heart rhythm disorder as assessed by ECG monitoring (Figure E4C and E5A-F). Using MRI, we also found that CS and poly(I:C)-exposition did not alter RV or LV volumes (Figure E4D-F). However, we detected a significant increase of RV wall thickness in exposed mice, indicating a RV hypertrophy (Figure 1L-M). This finding was confirmed by the measurement of the Fulton index (Figure 1N). Of note, the RV systolic pressure (RVSP) did not differ between early COPD and control mice (Figure 1O).

CXCR4 and CXCL12 expression is increased in blood and lung, respectively, in experimental early COPD and in patients with COPD

We next investigated the expression of CXCR4 and CXCL12 in blood and lung of mice and humans. The percentage of CXCR4-expressing cells was significantly increased in the blood of CS and poly(I:C)-exposed mice compared to control mice, 1 day after the last poly(I:C) instillation (Figure 2A-B). This effect appeared to be due to a synergy between CS and poly(I:C) (Figure E4). The level of $CXCR4^+$ circulating cells decreased and became similar between control and exposed mice 4 days after the last poly(I:C) instillation (Figure 2B). No significant modification of CXCL12 plasma concentration was evidenced (Figure 2C). The percentage of CXCR4-expressing cells was not significantly altered in whole lung homogenates in experimental early COPD (Figure 2D-E). However, CS and poly(I:C)-exposure significantly increased CXCL12 protein levels in lung homogenates, compared to control mice, 1 and 4 days after the last poly(I:C) instillation (Figure 2F).

To analyze the relevance of our findings to human disease, we determined whether CXCR4 expression was altered in patients with COPD by interrogating pre-existing RNAseq data from whole blood of control subjects and COPD patients (GSE100153 data set, http://www.ncbi.nlm.nih.gov/geo/). CXCR4 was significantly increased, at the mRNA level, in whole blood from patients with COPD compared to control subjects (Figure 2G). In a separate cohort of moderate to mild COPD patients (GOLD I to II, as defined by (1), Table E1), the percentage of CXCR4-expressing cells was also increased in the blood of moderate COPD patients in comparison with mild COPD patients (Figure 2H-I). In the lung, CXCR4 level was not significantly altered in patients with COPD compared to control smokers at the mRNA level

(GSE76925 data set, Figure 2J), which was corroborated by a similar result at the protein level (Figure 2K-L) in a separate cohort of patients with and without COPD (Table E2). In good agreement with our findings in mouse lungs, we also found a significant increased CXCL12 expression in patients with COPD (GSE76925 data set, Figure 2M), although we were not able to confirm it at the protein level (Figure 2N). In both human and mouse lungs, CXCL12 was predominantly localized to bronchial epithelial cells and peri-bronchial infiltrating cells, which are likely immune cells (Figure 2O-P). The CXCL12 immunostaining was markedly increased in lungs of animals exposed to CS and poly-(I:C) and lungs of patients with early COPD in comparison to control lungs (Table E3). CXCR4 was similarly expressed in COPD and control patients, mainly in inflammatory cells (Figure E7A). The density of $CXCR4^+$ cells in peri-bronchial area was unchanged in COPD patients compared to control subjects (Figure E7B).

Fibrocytes and $CXCR4^+$ fibrocytes are increased in lungs of experimental early COPD

The percentage of fibrocytes, defined as cells expressing CD45 and a high level of FSP1 ("$CD45^+$ $FSP1^{high}$") (21), was significantly increased in CS and poly(I:C)-exposed lungs, 1 day after the last poly(I:C) instillation (Figure 3A-C). In control and experimental early COPD, a vast majority of lung fibrocytes expressed CXCR4 (96.1 and 96.6 %, respectively, Figure 3B) and the percentage of $CXCR4^+$ fibrocytes was also significantly increased in the lungs of exposed mice (Figure 3D). The average percentage of leukocytes ($CD45^+$ cells) in control and exposed lungs was 69.2 % and 74.0 %, respectively (p=0.07, Figure 3E) whereas the percentage of fibrocytes ($CD45^+$ $FSP1^{high}$ cells) was 3.0% and 4.6%, respectively (p=0.002, Figure 3C). Four days after the last poly(I:C) instillation, the total level of fibrocytes decreased and became similar between control and experimental early COPD lungs (Figure 3C). Since the flow cytometry approach limits our analysis to the whole lung, we co-stained FSP1 with CD45 in murine lungs, 4 days after the last poly(I:C)

instillation (Figure 3F) using immunohistochemistry. Similarly to what we previously reported in human lung (14), the density of peri-bronchial fibrocytes was higher in CS and poly(I:C)-exposed mice lungs (median = 141 cells/mm^2 (95% CI, 128 to 321)) than in control mice (median = 92 cells/mm^2 (95% CI, 66 to 162)), p=0.049) (Figure 3G). Moreover, we also observed *in situ* CXCR4-expressing fibrocytes in peri-bronchial areas of human lung samples (Figure 3H).

CXCR4 deletion protects against functional airway obstruction, lung and heart tissue remodeling, and inhibits fibrocyte recruitment into the lungs in experimental early COPD

As mice genetically deficient for CXCR4 die perinatally (22), we generated conditional CXCR4 mutants using floxed allele (15) and a Cre2ERT2 strain (16), thereby obtaining mutants harboring a specific inactivation of CXCR4 at early adulthood after tamoxifen treatment. Intraperitoneal tamoxifen administration, for 5 consecutive days, in CXCR4$^{lox/lox}$/Cre2ERT2 mice was not sufficient to induce a large CXCR4 downregulation, in particular in the lungs (Figure E8A-B). Therefore, we combined intraperitoneal tamoxifen administration and feeding mice with tamoxifen-containing food to obtain robust decrease in CXCR4 expression in the lung and bone marrow (Figure E8C-E). As tamoxifen-containing food reduced weight gain in mice (Figure E2C-D), we used CXCR4$^{lox/lox}$ mice as control mice, and gave to all the transgenic mice tamoxifen-containing food. CXCR4$^{lox/lox}$/Cre2ERT2 were exposed to CS and poly(I:C) for 10 weeks, while control CXCR4$^{lox/lox}$ mice were exposed to either CS and poly(I:C), or normal air and PBS, thus generating three different mice groups (Figure 4A).

As expected, in CXCR4$^{lox/lox}$/Cre2ERT2 mice (CXCR4$^{-/-}$ mice), CXCR4 expression did not increase in the lung and blood (Figure E9). Moreover, FEV0.05/FVC ratio was higher in CXCR4$^{-/-}$ mice compared to CS and poly(I:C) CXCR4$^{lox/lox}$ mice (Figure 4B). The improvement in lung function in CXCR4$^{-/-}$ mice was confirmed by a significant decrease in the percentage of obstructive

mice (Figure 4C). The total number of cells in the BAL fluid, and its composition, were unchanged by CXCR4 deletion (Figure 4D-F). $CXCR4^{-/-}$ mice had a significant reduction in collagen deposition around small airways, compared to CS and poly(I:C)-exposed $CXCR4^{+/+}$ mice (Figure 4G-H), confirming an important role of CXCR4 in CS-induced bronchial remodeling.

We then assessed the impact of CXCR4 deletion on right heart remodeling. CXCR4 deletion did not affect hemodynamic and electrophysiological properties (Figure E10 and E5G-L) but it completely prevented the development of RV hypertrophy in exposed mice (Figure 4I-K). $CXCR4^{-/-}$ exposed mice had a similar value of Fulton index to that of unexposed mice (Figure 4J-K). RVSP value was unchanged between the three groups of mice (Figure 4L).

Moreover, we observed reduced flow cytometry levels of $CXCR4^{+}$ fibrocytes in CS and poly(I:C)-exposed whole lungs of $CXCR4^{-/-}$ mice compared with $CXCR4^{+/+}$ exposed mice, 1 day after the last poly(I:C) instillation (Figure 5A-D). Four days after the last poly(I:C) instillation, the density of fibrocytes was also significantly decreased around the small airways (Figure 5F-G).

Pharmacological inhibition of CXCR4 protects against functional obstruction and inhibits fibrocyte recruitment into the lungs in experimental COPD

We then assessed the efficacy of a CXCR4 antagonist (*i.e.*, plerixafor) in the present murine model (Figure 6A). Mice weight was not affected by daily subcutaneous plerixafor treatment during the second half of the protocol (Figure E2E-F). Plerixafor significantly reduced CXCR4 expression 1 day after the last poly(I:C) instillation in circulating cells, but not in lung cells (Figure E11). In CS and poly(I:C)-exposed-mice treated with plerixafor, the FEV0.05/FVC ratio and the percentage of obstructive mice were significantly increased and decreased, respectively, in comparison with vehicle-treated exposed mice (Figure 6A-C). As a result, CS and poly(I:C)-exposed mice with drug treatment had similar a lung function to that of RA and PBS-exposed controls. The total number

of cells in the BAL fluid and its composition was unchanged by plerixafor treatment (Figure 6D-F). The peri-bronchial fibrosis was slightly, although not significantly, decreased in plerixafor treated lungs (Figure 6G-H). To identify pathways that were differentially regulated by the early COPD protocol and plerixafor treatment, we performed proteome analysis on lungs obtained 1 day after the last poly-IC instillation. Comparison analysis revealed a significant inhibition of pathways of inflammation, cell invasion, movement, adhesion and synthesis of reactive oxygen species (ROS) in relation to plerixafor treatment (Figure 6K). These changes were driven by down-regulation of a core set of proteins such as thioredoxin interacting protein (TXNIP), matrix metalloproteinase-8 (MMP-8) and vimentin (Figure E12).

Moreover, we assessed the effect of plerixafor on right heart remodeling. Treatment with plerixafor reduced the development of RV hypertrophy in exposed mice, as shown by a significant decrease of the Fulton index (Figure 6I). The RVSP, as well as heart electrophysiological properties remained unchanged by CXCR4 inhibition (Figure 6J, S5M-R).

Finally, we examined infiltrating $CD45^+$ $FSP1^{high}$ cells and $CD45^+$ $FSP1^{high}$ $CXCR4^+$cells by flow cytometry 1 day after the last poly(I:C) instillation. Our results showed that both the number of fibrocytes and $CXCR4^+$ fibrocytes significantly decreased in plerixafor-treated-CS and poly(I:C)-exposed lungs compared to vehicle-treated lungs (Figure E13A-D). Four days after the last poly(I:C) instillation, the density of peri-bronchial fibrocytes was significantly reduced by plerixafor treatment (Figure E13F-G).

DISCUSSION

We designed the present dedicated murine model of early COPD to examine pathophysiological processes at the onset of the disease. We have demonstrated that the CXCL12/CXCR4 axis plays

a major role in the pathogenesis of lung and heart remodeling. Indeed, both genetic silencing and pharmacological inhibition of CXCR4 in this experimental early COPD model reduced both the level of CXCR4-expressing cells in the peripheral circulation and fibrocyte recruitment into the lungs, along with a proteomic signature consistent with decreased inflammation. As a consequence, CXCR4 inhibition prevented CS-induced lung and cardiac remodeling, as well as airflow limitation. Finally, for translational purpose, we also showed that CXCR4 was increased in the blood of patients even with a mild COPD whereas CXCL12 was increased in the lung of early COPD patients.

We set up the present murine model of early COPD based on the following. First, 10-week old mice exposed to CS for 10 weeks would correspond to young human adults chronically exposed to tobacco smoke for several years (23) and, second, as in humans, exposed mice exhibited limited but significant airflow limitation together with both neutrophilic/lymphocytic airway inflammation and distal airway remodeling, but without obvious signs of alveolar destructions (24). By contrast, the vast majority of mice COPD models are based on long term CS exposure (up to 6 months) either mimicking emphysema, or reproducing severe airway obstruction together with emphysema-like changes (25). Moreover, we used a combination of CS exposure with poly-(I:C) as a TLR3 agonist to mimic respiratory viral infections (18), which are more frequent in smokers (26). Finally, the present model also includes features of early RV hypertrophy (27), without established pulmonary hypertension, as previously identified in a long term murine model (28), thus confirming again the relevance of this animal model of early COPD. Extra pulmonary effects, such as cardiovascular diseases, are indeed frequently seen in current smokers (29) and patients with COPD (30), and they contribute to the high levels of COPD morbidity, mortality and health-care costs.

A main result of the present study is the increase of CXCL12 expression in the lungs of early COPD mice and patients, along with an increase in CXCR4 positive cells in the blood of early COPD mice as well as in COPD patients. Treating mice with the CXCR4 antagonist plerixafor prevented the increase of CXCR4-expressing cells, attenuated tissue fibrocytes recruitment and lung function degradation. Targeting CXCR4 with daily injections of plerixafor during the 5 last weeks of the protocol as well as genetic deletion of CXCR4 also decreased CS and poly-(I:C) induced-right heart remodeling. In this connection, neutralizing CXCL12 or antagonizing CXCR4 has been previously shown to attenuate RV hypertrophy in a rat model of severe pulmonary hypertension (31). The fact that the beneficial effect on lung function and remodeling in plerixafor-treated mice, exhibiting increased CXRCR4 solely in the blood, was similar with that observed in $CXCR4^{-/-}$ mice suggests that such beneficial effect occurred through CXCR4 reduction in the blood rather than in the lungs. These results are in agreement with findings obtained in mice treated with another CXCR4 antagonist or with CXCL12 neutralizing antibodies, in the context of pulmonary fibrosis, where reduction of fibrocytes accumulation concomitantly improved lung outcomes (13, 32). The reduction of tissue fibrocytes could thus contribute to lower chronic inflammation (33). Finally, plerixafor-induced increased mobilization of hematopoietic progenitor cells from the bone marrow may also participate in the improvement of lung function and remodeling as suggested by another study showing that plerixafor-treated mice were protected against CS-induced emphysema (12). It is noteworthy that we did not assess the mechanisms of blood CXCR4 increase even though several mechanisms of up-regulation may be proposed, including effects mediated by mild/intermittent hypoxia (9), the Vascular Endothelial Growth Factor (VEGF) et the basic Fibroblast Growth Factor (bFGF), described in endothelial cells (34), or IL-33, described in fibrocytes (35, 36).

CONCLUSION

Collectively, our data in both a murine model and in humans, indicate that the CXCL12/CXCR4 axis plays an important role in the pathogenesis of early COPD. Inhibition of such axis, as shown in the present murine model, improves lung function and decreases cardiac comorbidities, thus opening new therapeutic options in this progressive and devastating disease, supporting the future use of CXCR4 inhibitors for early COPD treatment, that might slow down the progression of the disease.

ACKNOWLEDGEMENTS

We thank the study participants and the staff of the Thoracic Surgery, Radiology, Pathology, Respiratory, Lung Function Testing departments from the University Hospital of Bordeaux (Bordeaux, France), Fabienne Estella for technical assistance with mice protocol, Isabelle Goasdoue, Isabelle Bernis, Natacha Robert, Virginie Niel, and Marine Servat from the clinical investigation center for technical assistance, and Atika Zouine and Vincent Pitard for technical assistance at the Flow cytometry facility (CNRS UMS 3427, INSERM US 005, Univ. Bordeaux, F-33000 Bordeaux, France), Anne-Aurélie Raymond for help with proteomic analysis at the Oncoprot Platform (TBMCore US005). Christel Poujol, Sébastien Marais and Fabrice Cordelières for help with imaging and image analysis et the Bordeaux Imaging Centre (BIC; Bordeaux, France). Microscopy was performed at BIC, a service unit of the CNRS-INSERM and Bordeaux University, a member of the national BioImaging infrastructure of France supported by the French National Research Agency (ANR-10-INBS-04).

DATA SHARING

Qualified researchers can request access to all data through the corresponding author.

REFERENCES

1. Global Initiative for Chronic Obstructive Lung Disease. *Global Initiative for Chronic Obstructive Lung Disease - GOLD* at <https://goldcopd.org/>.
2. Mannino DM, Buist AS. Global burden of COPD: risk factors, prevalence, and future trends. *Lancet* 2007;370:765–773.
3. Martinez FJ, Han MK, Allinson JP, Barr RG, Boucher RC, Calverley PMA, *et al.* At the Root: Defining and Halting Progression of Early Chronic Obstructive Pulmonary Disease. *Am J Respir Crit Care Med* 2018;197:1540–1551.
4. Çolak Y, Afzal S, Nordestgaard BG, Lange P, Vestbo J. Importance of Early COPD in Young Adults for Development of Clinical COPD: Findings from the Copenhagen General Population Study. *Am J Respir Crit Care Med* 2021;203:1245–1256.
5. Cosío BG, Casanova C, Soler-Cataluña JJ, Soriano JB, García-Río F, Lucas P de, *et al.* Unravelling young COPD and pre-COPD in the general population. *ERJ Open Research* 2023;9:.
6. Henrot P, Prevel R, Berger P, Dupin I. Chemokines in COPD: From Implication to Therapeutic Use. *Int J Mol Sci* 2019;20:.
7. Dupin I, Allard B, Ozier A, Maurat E, Ousova O, Delbrel E, *et al.* Blood fibrocytes are recruited during acute exacerbations of chronic obstructive pulmonary disease through a CXCR4-dependent pathway. *J Allergy Clin Immunol* 2016;137:1036-1042.e7.
8. Busillo JM, Benovic JL. Regulation of CXCR4 signaling. *Biochimica et Biophysica Acta (BBA) - Biomembranes* 2007;1768:952–963.
9. Schioppa T, Uranchimeg B, Saccani A, Biswas SK, Doni A, Rapisarda A, *et al.* Regulation of the Chemokine Receptor CXCR4 by Hypoxia. *Journal of Experimental Medicine* 2003;198:1391–1402.

10. Tian X, Xie G, Xiao H, Ding F, Bao W, Zhang M. CXCR4 knockdown prevents inflammatory cytokine expression in macrophages by suppressing activation of MAPK and NF-κB signaling pathways. *Cell & Bioscience* 2019;9:55.
11. Petty JM, Sueblinvong V, Lenox CC, Jones CC, Cosgrove GP, Cool CD, *et al.* Pulmonary stromal-derived factor-1 expression and effect on neutrophil recruitment during acute lung injury. *J Immunol* 2007;178:8148–8157.
12. Barwinska D, Oueini H, Poirier C, Albrecht ME, Bogatcheva NV, Justice MJ, *et al.* AMD3100 ameliorates cigarette smoke-induced emphysema-like manifestations in mice. *Am J Physiol Lung Cell Mol Physiol* 2018;315:L382–L386.
13. Phillips RJ, Burdick MD, Hong K, Lutz MA, Murray LA, Xue YY, *et al.* Circulating fibrocytes traffic to the lungs in response to CXCL12 and mediate fibrosis. *J Clin Invest* 2004;114:438–446.
14. Dupin I, Thumerel M, Maurat E, Coste F, Eyraud E, Begueret H, *et al.* Fibrocyte accumulation in the airway walls of COPD patients. *Eur Respir J* 2019;54:.
15. Tokoyoda K, Egawa T, Sugiyama T, Choi B-I, Nagasawa T. Cellular Niches Controlling B Lymphocyte Behavior within Bone Marrow during Development. *Immunity* 2004;20:707–718.
16. Jullien N, Goddard I, Selmi-Ruby S, Fina J-L, Cremer H, Herman J-P. Use of ERT2-iCre-ERT2 for conditional transgenesis. *Genesis* 2008;46:193–199.
17. Almolki A, Guenegou A, Golda S, Boyer L, Benallaoua M, Amara N, *et al.* Heme oxygenase-1 prevents airway mucus hypersecretion induced by cigarette smoke in rodents and humans. *Am J Pathol* 2008;173:981–992.

18. Kang M-J, Lee CG, Lee J-Y, Dela Cruz CS, Chen ZJ, Enelow R, *et al.* Cigarette smoke selectively enhances viral PAMP- and virus-induced pulmonary innate immune and remodeling responses in mice. *J Clin Invest* 2008;118:2771–2784.
19. Esteves P, Blanc L, Celle A, Dupin I, Maurat E, Amoedo N, *et al.* Crucial role of fatty acid oxidation in asthmatic bronchial smooth muscle remodelling. *Eur Respir J* 2021;58:2004252.
20. Hogg JC, McDonough JE, Sanchez PG, Cooper JD, Coxson HO, Elliott WM, *et al.* Micro–Computed Tomography Measurements of Peripheral Lung Pathology in Chronic Obstructive Pulmonary Disease. *Proc Am Thorac Soc* 2009;6:546–549.
21. Sangaletti S, Tripodo C, Cappetti B, Casalini P, Chiodoni C, Piconese S, *et al.* SPARC oppositely regulates inflammation and fibrosis in bleomycin-induced lung damage. *Am J Pathol* 2011;179:3000–3010.
22. Tachibana K, Hirota S, Iizasa H, Yoshida H, Kawabata K, Kataoka Y, *et al.* The chemokine receptor CXCR4 is essential for vascularization of the gastrointestinal tract. *Nature* 1998;393:591–594.
23. Dutta S, Sengupta P. Men and mice: Relating their ages. *Life Sciences* 2016;152:244–248.
24. Higham A, Quinn AM, Cançado JED, Singh D. The pathology of small airways disease in COPD: historical aspects and future directions. *Respir Res* 2019;20:49.
25. Tanner L, Single AB. Animal Models Reflecting Chronic Obstructive Pulmonary Disease and Related Respiratory Disorders: Translating Pre-Clinical Data into Clinical Relevance. *JIN* 2020;12:203–225.
26. Arcavi L, Benowitz NL. Cigarette Smoking and Infection. *Archives of Internal Medicine* 2004;164:2206–2216.

27. Hilde JM, Skjørten I, Grøtta OJ, Hansteen V, Melsom MN, Hisdal J, *et al.* Right ventricular dysfunction and remodeling in chronic obstructive pulmonary disease without pulmonary hypertension. *J Am Coll Cardiol* 2013;62:1103–1111.
28. Weissmann N, Lobo B, Pichl A, Parajuli N, Seimetz M, Puig-Pey R, *et al.* Stimulation of soluble guanylate cyclase prevents cigarette smoke-induced pulmonary hypertension and emphysema. *Am J Respir Crit Care Med* 2014;189:1359–1373.
29. Banks E, Joshy G, Korda RJ, Stavreski B, Soga K, Egger S, *et al.* Tobacco smoking and risk of 36 cardiovascular disease subtypes: fatal and non-fatal outcomes in a large prospective Australian study. *BMC Medicine* 2019;17:128.
30. Chen W, Thomas J, Sadatsafavi M, FitzGerald JM. Risk of cardiovascular comorbidity in patients with chronic obstructive pulmonary disease: a systematic review and meta-analysis. *Lancet Respir Med* 2015;3:631–639.
31. Bordenave J, Thuillet R, Tu L, Phan C, Cumont A, Marsol C, *et al.* Neutralization of CXCL12 attenuates established pulmonary hypertension in rats. *Cardiovasc Res* 2019;doi:10.1093/cvr/cvz153.
32. Griffiths K, Habiel DM, Jaffar J, Binder U, Darby WG, Hosking CG, *et al.* Anti-fibrotic Effects of CXCR4-Targeting i-body AD-114 in Preclinical Models of Pulmonary Fibrosis. *Sci Rep* 2018;8:3212.
33. Eyraud E, Maurat E, Sac-Epée J-M, Henrot P, Zysman M, Esteves P, *et al.* Short-range interactions between fibrocytes and CD8+ T cells in COPD bronchial inflammatory response. 2022;doi:10.1101/2022.10.21.513138.
34. Salcedo R, Wasserman K, Young HA, Grimm MC, Howard OM, Anver MR, *et al.* Vascular endothelial growth factor and basic fibroblast growth factor induce expression of CXCR4 on

human endothelial cells: In vivo neovascularization induced by stromal-derived factor-1alpha. *Am J Pathol* 1999;154:1125–1135.

35. Wang C-H, Weng C-M, Huang T-T, Lee M-J, Lo C-Y, Chen M-C, *et al.* Anti-IgE therapy inhibits chemotaxis, proliferation and transformation of circulating fibrocytes in patients with severe allergic asthma. *Respirology* 2021;doi:10.1111/resp.14096.
36. Berger P, Dupin I. Unravelling the effects of omalizumab on fibrocytes. *Respirology* 2021;26:825–827.
37. Dupin I, Henrot P, Maurat E, Eyraud E, Esteves P, Zysman M, *et al.* Targeting CXCR4 as a therapeutic strategy to improve outcomes in a mouse model of early chronic obstructive pulmonary disease (COPD). *ERJ Open Research* 2022;8:.
38. Dupin I, Dubreuil M, Freund-Michel V, Maurat E, Campagnac M, Ousova O, *et al.* Targeting CXCR4 as a therapeutic strategy to improve outcomes in a mouse model of early chronic obstructive pulmonary disease (COPD). *ERJ Open Research* 2019;5:.

FIGURE LEGENDS

Figure 1: Evaluation of lung function, inflammation, bronchial and heart remodeling in experimental COPD. A, Mice are exposed either to room air (RA) and challenged with PBS, or exposed to cigarette smoke (CS) and challenged with poly(I:C), during 10 weeks. They are sacrificed at day 68 or 71 (i.e. 1 day or 4 days after the last poly(I:C) instillation). B, Average expiratory flow-volume curves of RA+PBS-exposed mice (black curve) and CS+poly(I:C)-exposed mice (gray curve). Lower and upper error bars represent standard deviations for CS+poly(I:C) and RA+PBS-exposed mice, respectively. C, FEV0.05/FVC (FEV0.05: Forced Expiratory Volume during 0.05 s, FVC: Forced Vital Capacity) of RA+PBS-exposed mice (black circles, lower 95% confidence interval (CI) of the mean: 0.837) and CS+poly(I:C)-exposed mice (gray squares). Data represent individual mice. D, Percentage of obstructive mice, defined as mice with FEV0.05/FVC<0.837. Fisher's test. E, Total cell count in bronchoalveolar lavage (BAL). Kruskal-Wallis test followed by Dunn's post-tests. F-I, BAL differential cell recovery 1 day (F, H) and 4 days (G, I) after the last poly(I:C) instillation. H, Top Canonical Ingenuity Pathways significantly altered in CS+poly(I:C) (n=5) *vs* RA+PBS (n=5)-exposed lungs (n=5) obtained 1 day after the last poly-IC instillation, ranked by Z-score (negative and positive for the pathways represented respectively on the top and bottom part of the graph), obtained by Gene Set Enrichment Analysis. I, Heatmaps of differentially regulated proteins in CS+poly(I:C) vs RA+PBS-exposed lungs, from the pathways "hypercytokinemia/hyperchemokinemia in the pathogenesis of influenza" (left), "wound healing signaling pathway" (middle) and "xenobiotic metabolism PXR signaling pathway" (right). The color scale indicates the $\log_2$ fold changes of abundance for each protein. J, Representative Masson's trichrome stainings to assess peri-bronchial fibrosis. K, Standardized fibrosis, defined as (peri-bronchial fibrosis ("PF", %) - mean PFcontrol)/standard deviation PFcontrol). The peri-bronchial fibrosis ("PF", percentage) is defined by the ratio between

the area of segmented pixels in the area of analysis divided by the total peri-bronchial area. L, Representative short-axis cine magnetic resonance images of heart at end-systolic stage (left panels) and end-diastolic stage (middle panels) in control mice (top panels) and CS and poly(I:C)-exposed mice (bottom panels). Right panels: higher magnification of RV wall. M, Wall thickness. N, Fulton index, defined as (right ventricle (RV)/ left ventricle plus septum (LV + S). O, Right ventricular systolic pressure (RVSP). C, F, G, K, M, N, O, Unpaired t test or Mann-Whitney test. *: $P<0.05$, **: $P<0.01$, ***: $P<0.001$.

Figure 2: Characterization of CXCR4 and CXCL12 expression in the blood and lung in experimental COPD and in patients with or without COPD. A-F, O, Mice are exposed either to room air (RA) and challenged with PBS, or exposed to cigarette smoke (CS) and challenged with poly(I:C), during 10 weeks. They are sacrificed at day 68 or 71 (i.e. 1 day or 4 days after the last poly(I:C) instillation). A, D, H, Upper left panels: dot plots represent representative side scatter (SSC, y-axis)-forward scatter (FSC, x-axis) graphs of circulating (A, H) and lung (F) cells. $DAPI^-$ cells, and $DAPI^-$ $CXCR4^+$ cells are shown respectively in gray and pink. Upper right panels and bottom panels: histograms represent representative cell count (y-axis) versus Phycoerythrin (PE) fluorescence (x-axis) in $DAPI^-$ circulating (A, H) and lung (D) cells. Percentages of $CXCR4^+$ cells in the $DAPI^-$ cells are shown in pink. B, E, Levels of circulating (C) and lung (H) $CXCR4^+$ cells 1 day (d+1) and 4 days (d+4) after the last poly(I:C) instillation. C, F, Plasma (C) and lung (F) CXCL12 concentration at d+1 and d+4. For lung CXCL12 concentration, the value is normalized to total protein concentration. G, CXCR4 mRNA expression in whole blood. Data are derived from a publicly available GSE-set (GSE100153). Control subjects n=24; patients with COPD n=19. I, Levels of circulating $CXCR4^+$ cells in patients with moderate COPD (GOLD I, defined by forced expiratory volume in 1 second (FEV1) $\geq$ 80% predicted, n=5) and mild COPD (GOLD II, defined by 50% $\leq$ FEV1 < 80% predicted, n=5). J, M, CXCR4 (J) and CXCL12 (M) mRNA expression in human lungs. Data are derived from a publicly available GSE-set (GSE76925). Control subjects n=40; patients with COPD n=111. K, L, N Immunoblot assay of CXCR4 protein expression levels (K), its quantification (L) and CXCL12 levels (measured by ELISA, N) in lung samples from control subjects (n=4) and patients with COPD (n=4). Stain free gel technology has been used for loading control expression quantification. For lung CXCL12 concentration, the value is normalized to total protein concentration. O, P, Representative stainings of CXCL12 (magenta) and nucleus (blue) in peri-bronchial areas of mouse (O) and human (P) lungs. Lower panels: higher

magnification of the images surrounded by white squares in the upper panels. Images obtained in RA and PBS *vs* CS and poly(I:C)-exposed mice and in control *vs* early COPD lungs have been acquired with the same exposure time and gain. The white arrowheads and arrows indicate respectively CXCR4-expressing bronchial cells and immune-type cells. B, C, E, F, G, I, J, L, M, N, Medians are represented as horizontal lines. *: P <0.05, **: P<0.01, ***: P<0.001, Mann-Whitney test.

Figure 3: Characterization of lung fibrocyte level and localization in experimental COPD and in patients with or without COPD. A-G, Mice are exposed either to room air (RA) and challenged with PBS, or exposed to cigarette smoke (CS) and challenged with poly(I:C), during 10 weeks. They are sacrificed 1 day ("d+1") or 4 days ("d+4") after the last poly(I:C) instillation. A, Representative flow cytometry contour plots in each condition. The x-axis is for CD45-Allophycocyanin (APC) fluorescence and the y-axis, FSP1-Fluorescein-5-isothiocyanate (FITC) fluorescence. Percentages of $CD45^+$ $FSP1^{high}$ cells are shown in green. B, Representative cell count (y-axis) versus CXCR4-Phycoerythrin (PE) fluorescence (x-axis) in $CD45^+$ $FSP1^{high}$-cell subsets in mouse lungs. C-E, Levels of lung $CD45^+$ $FSP1^{high}$ cells (C), $CD45^+$ $FSP1^{high}$ $CXCR4^+$ cells (D), $CD45^+$ cells (E), in RA+PBS-exposed mice (black circles) and CS+poly(I:C)-exposed mice (gray squares), at d+1 and d+4. F, Representative stainings of CD45 (green) and FSP1 (red) in peri-bronchial areas (delimited in pink) of lung mice at d+4. The white arrows indicate fibrocytes, defined as $CD45^+$ $FSP1^+$ cells. G, Quantification of fibrocyte density (normalized by peri-bronchial area). H, Representative stainings of CD45 (green) and FSP1 (red) in peri-bronchial area. The white arrowheads indicate fibrocytes, defined as $CD45^+$ $FSP1^+$ cells. F, Representative stainings of CD45 (green), FSP1 (red), nuclei (DAPI, blue) and CXCR4 (white) in peri-bronchial areas of lung samples of control subjects and patients with COPD. The white arrows indicate CXCR4-expressing fibrocytes, defined as $CD45^+$ $FSP1^+$ $CXCR4^+$ cells. F, H, Left and lower panels: higher magnification of the images surrounded by white squares in the right upper panels. C-E, G, Medians are represented as horizontal lines. *: $P < 0.05$, **: $P < 0.01$, Mann-Whitney test.

Figure 4: Evaluation of lung function, inflammation and bronchial and heart remodeling upon conditional knockout of CXCR4 in experimental COPD. A, $CXCR4^{lox/lox}$ mice are exposed either to room air (RA) and challenged with PBS (black curve/bar/circles) or to cigarette smoke (CS) and challenged with poly(I:C) (gray curve/bar/squares). $CXCR4^{lox/lox}$/Cre2ERT2 mice are exposed to cigarette smoke (CS) and challenged with poly(I:C) (pink curve/bar/squares). All the mice were administered with 1 mg intraperitoneal tamoxifen for 5 consecutive days at the beginning of the COPD protocol, and then fed by tamoxifen-containing food during the remaining protocol. They are sacrificed at day 68 or 71 (1 day and 4 days after the last poly(I:C) instillation). B, FEV0.05/FVC in the different conditions. Control condition, lower 95% confidence interval (CI) of the mean: 0.8237. Data represent individual mice. C, Percentage of obstructive mice, defined as mice with FEV0.05/FVC<0.8237. Fisher's test. D, Total cell count in bronchoalveolar lavage (BAL). E-F, BAL relative (E) and absolute (F) cell composition respectively 1 day and 4 days after the last poly(I:C) instillation. G, Representative Masson's trichrome stainings to assess peri-bronchial fibrosis. H, Standardized fibrosis, defined as (peri-bronchial fibrosis ("PF", %) - mean PFcontrol)/standard deviation PFcontrol). The peri-bronchial fibrosis ("PF", percentage) is defined by the ratio between the area of segmented pixels in the area of analysis divided by the total peri-bronchial area. I, Representative short-axis cine magnetic resonance images at end-systolic stage (left panels) and end-diastolic stage (middle panels) in CS and poly(IC)-exposed $CXCR4^{lox/lox}$ mice (top panels) and CS and poly(IC)-exposed $CXCR4^{lox/lox}$/Cre2ERT2 mice (bottom panels). Right panels: higher magnification of RV wall. J, Wall thickness. **: P<001, Mann-Whitney test. K, Fulton index, defined as (right ventricle (RV)/ left ventricle plus septum (LV + S). L, Right ventricular systolic pressure (RVSP). B, D, E, F, H, K, L, *: P<0.05, **: P<0.01, ***: P<0.001. Kruskal-Wallis test followed by Dunn's post-tests.

Figure 5: Characterization of fibrocyte level and peri-bronchial density in lung upon conditional knockout of CXCR4 in experimental COPD. $CXCR4^{lox/lox}$ mice are exposed either to room air (RA) and challenged with PBS (black circles) or to cigarette smoke (CS) and challenged with poly(I:C) (gray squares). $CXCR4^{lox/lox}$/Cre2ERT2 mice are exposed to cigarette smoke (CS) and challenged with poly(I:C) (pink squares). They are sacrificed at day 68 or 71 (1 day and 4 days after the last poly(I:C) instillation). A, Representative flow cytometry contour plots in each condition. The x-axis is for CD45-Allophycocyanin (APC) fluorescence and the y-axis, FSP1-Fluorescein-5-isothiocyanate (FITC) fluorescence. Percentages of $CD45^+$ $FSP1^{high}$ cells are shown in green. B, Representative cell count (y-axis) versus CXCR4-Phycoerythrin (PE) fluorescence (x-axis) in $CD45^+$ $FSP1^{high}$-cell subsets in mouse lungs. C-E) Levels of lung $CD45^+$ $FSP1^{high}$ cells (C), $CD45^+$ $FSP1^{high}$ $CXCR4^+$ cells (D), $CD45^+$ cells (E) 1 day after the last poly(I:C) instillation in each condition. F, Quantification of fibrocyte density (normalized by peri-bronchial area) 4 days after the last poly(I:C) instillation in each condition. G, Representative stainings of CD45 (green) and FSP1 (red) in peri-bronchial area (delimited in pink) in each condition. The white arrows indicate fibrocytes, defined as $CD45^+$ $FSP1^+$ cells. C-F, Medians are represented as horizontal lines. *: $P < 0.05$, **: $P < 0.01$, one-way analysis of variance or Kruskal-Wallis test followed respectively by Bonferroni's or Dunn's post-tests.

Figure 6: Evaluation of lung function, inflammation and bronchial and heart remodeling upon pharmacological blockage of CXCR4 in experimental COPD. A, Mice are exposed either to room air (RA), challenged with PBS and treated by plerixafor's vehicle (black curve/bar/circles), or exposed to cigarette smoke (CS), challenged with poly(I:C) and treated with plerixafor ("pleri", 1 mg/kg, purple curve/bar/squares) or its vehicle (gray curve/bar/squares). They are sacrificed at day 68 or 71 (1 day and 4 days after the last poly(I:C) instillation). B, FEV0.05/FVC in the different conditions. Control condition, lower 95% confidence interval (CI) of the mean: 0.8099. Data represent individual mice. C, Percentage of obstructive mice, defined as mice with FEV0.05/FVC<0.8099. Fisher's test. D, Total cell count in bronchoalveolar lavage (BAL). E-F, BAL relative (E) and absolute (F) cell composition respectively 1 day and 4 days after the last poly(I:C) instillation. G, Representative Masson's trichrome stainings to assess peri-bronchial fibrosis. H, Standardized fibrosis, defined as (peri-bronchial fibrosis ("PF", %) - mean PFcontrol)/standard deviation PFcontrol). The peri-bronchial fibrosis ("PF", percentage) is defined by the ratio between the area of segmented pixels in the area of analysis divided by the total peri-bronchial area. I, Fulton index, defined as (right ventricle (RV)/ left ventricle plus septum (LV + S). J, Right ventricular systolic pressure (RVSP). K, Heatmaps of significantly differentially regulated pathways identified by Ingenuity Pathway analysis (IPA; Qiagen), obtained by proteomics comparison of CS+poly(I:C) (n=5) *vs* RA+PBS (n=5)-exposed lungs (n=5) (all treated by vehicle), and plerixafor (n=5) vs vehicle (n=5)-treated lungs (all exposed to CS+poly(I:C)). The color scale indicates the Z-score value. B, D, E, F, H, I, J, *: P<0.05, **: P<0.01, ***: P<0.001. Kruskal-Wallis test followed by Dunn's post-tests.

Footnote: Some of the results of this study have been previously reported in the form of an abstract (37, 38).

FIGURES

Figure 1

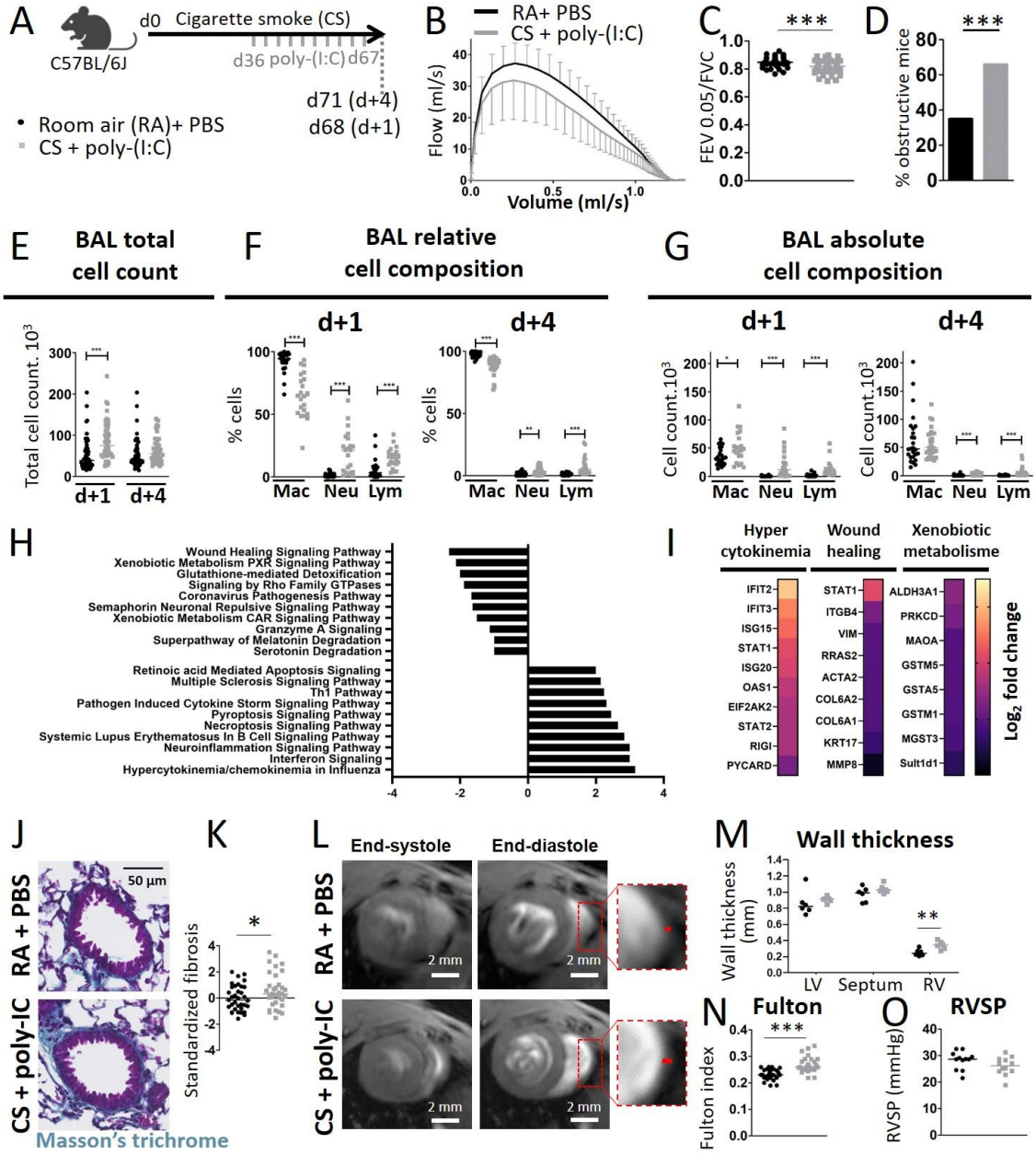

Figure 2

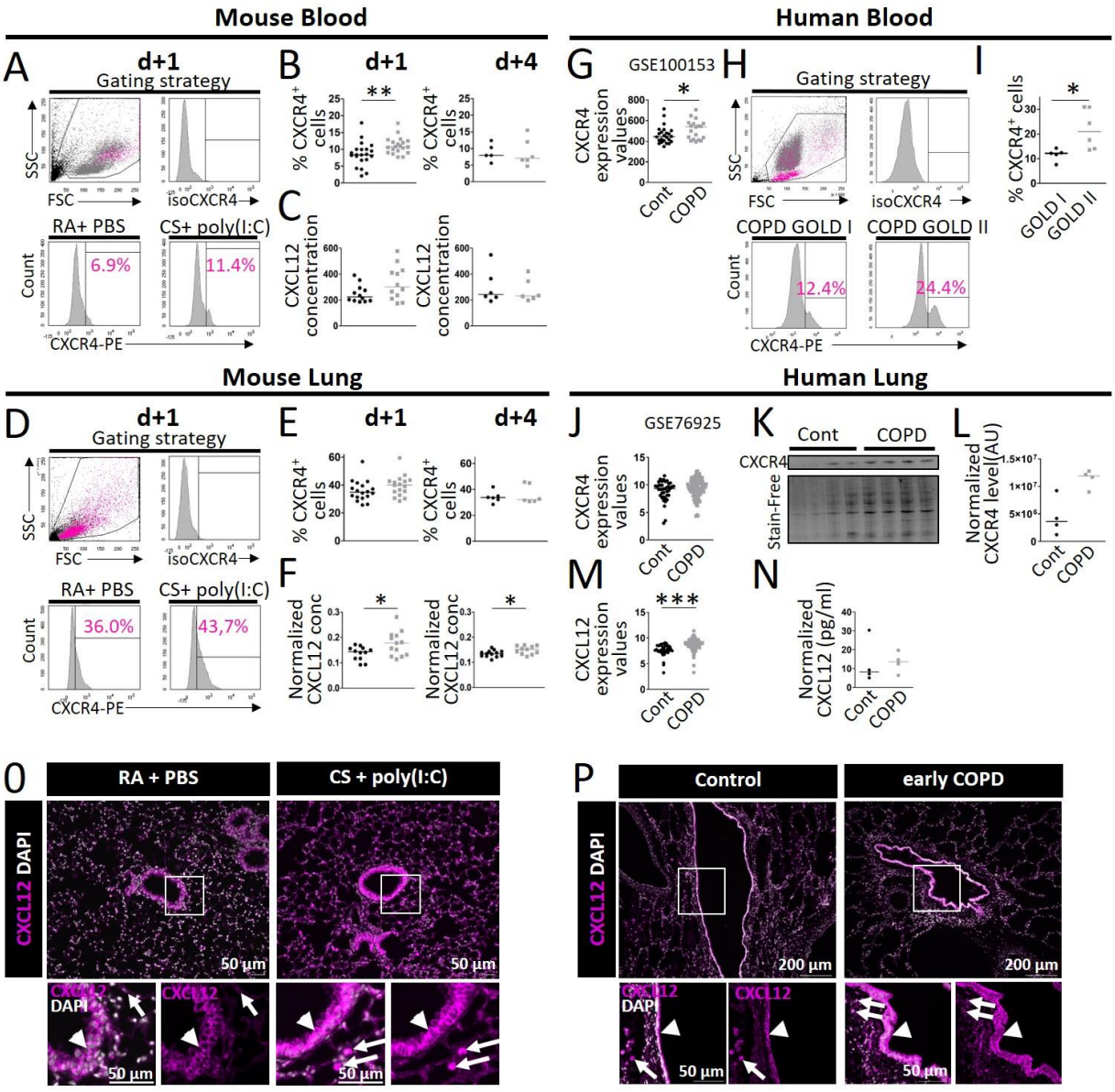

Figure 3

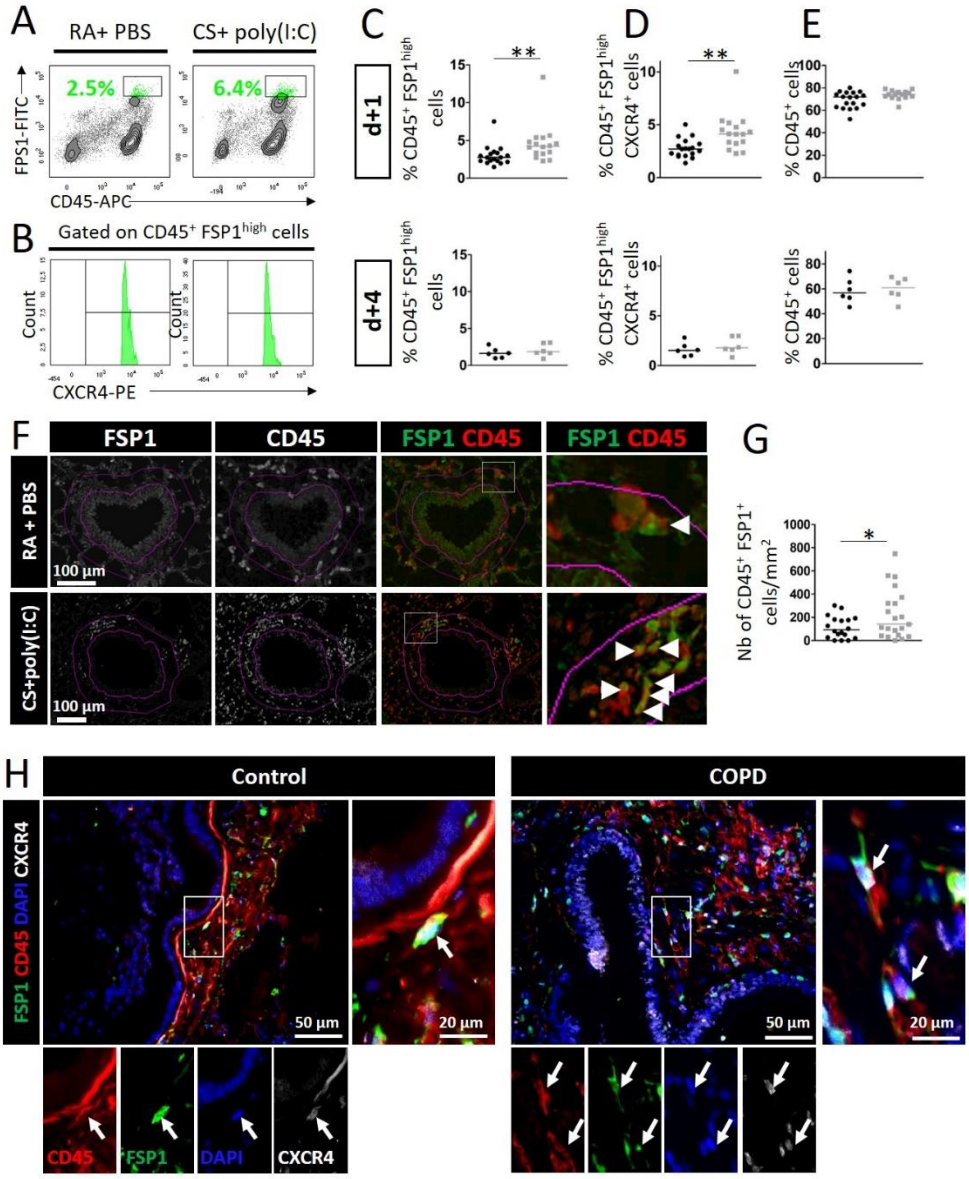

Figure 4

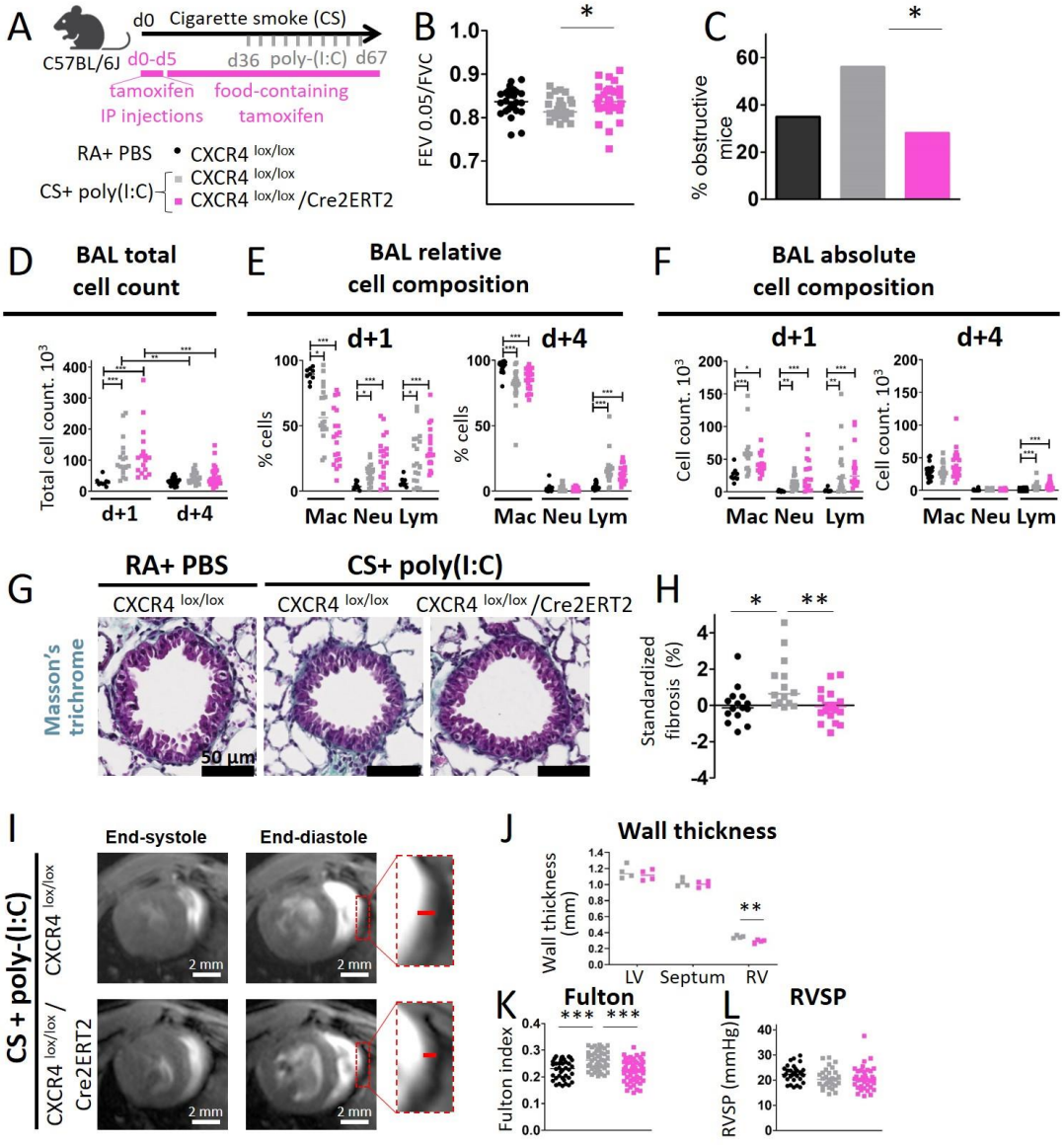

Figure 5

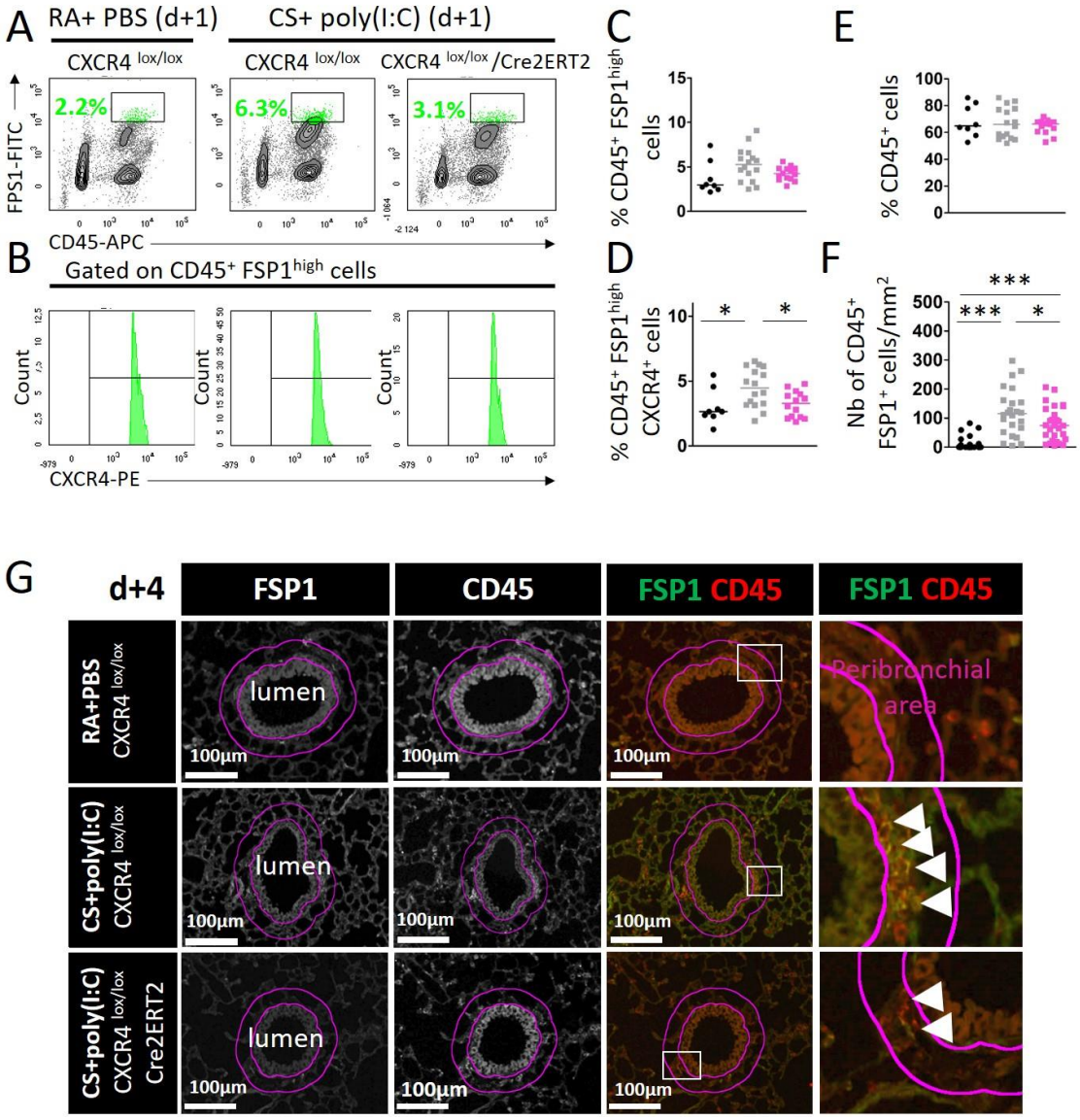

Figure 6